Journal of Colloid and Interface Science 564 (2020) 499–509

Contents lists available at ScienceDirect

Journal of Colloid and Interface Science

journal homepage: www.elsevier.com/locate/jcis

Exploring the gel phase of cationic glycylalanylglycine in ethanol/water. I. Rheology and microscopy studies

Lavenia J. Thursch [a], David DiGuiseppi [b], Todd R. Lewis [a], Reinhard Schweitzer-Stenner [b,*], Nicolas J. Alvarez [a,*]

[a] Department of Chemical and Biological Engineering, Drexel University, Philadelphia, PA 19104, USA
[b] Department of Chemistry, Drexel University, Philadelphia, PA 19104, USA

GRAPHICAL ABSTRACT

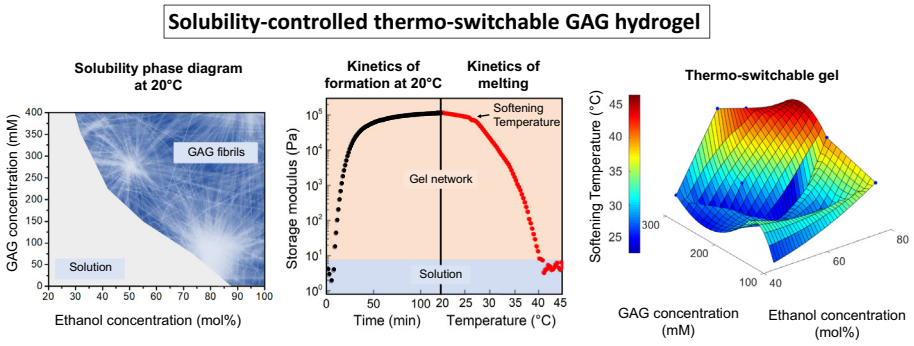

ARTICLE INFO

Article history:
Received 26 August 2019
Revised 7 October 2019
Accepted 8 October 2019
Available online 12 October 2019

Keywords:
Self-assembly
Peptide fibrils
GAG
Gelation kinetics
Gel rheology

ABSTRACT

Hypothesis: The cationic tripeptide glycylalanylglycine (GAG) self-assembles into long, thick crystalline fibrils in an ethanol/water solution. At sufficiently high concentrations, the fibrils form a volume spanning hydrogel network. We report an extensive rheology and microscopy-based study regarding the self-assembly of GAG in ethanol/water solutions to understand the conditions for fibril formation as well as the thermal stability for future developments of this material.

Experiments: By systematically varying GAG concentration and ethanol fraction, we observe a two-dimensional fibril aggregate phase diagram. Microscopy studies shed light on the shape and size of fibrils as well as the macroscopic packing depending on conditions. The kinetics and evolution of the macroscopic fibril microstructure was investigated using rheology.

Findings: The mechanism of fibril formation is put into the context of a solubility framework, where ethanol reduces peptide solubility and induces self-assembly. The rate of fibril formation and strength of the gel can be controlled by peptide concentration and ethanol fraction. The faster rate of fibril formation leads to inhomogeneous packing of fibrils denoted by discrete dense fibril clusters. The solubility of the fibrils can be manipulated by temperature making the gel thermo-switchable, a property of interest for biomedical systems.

© 2019 Elsevier Inc. All rights reserved.

* Corresponding authors.
E-mail addresses: rschweitzer-stenner@drexel.edu (R. Schweitzer-Stenner), nja49@drexel.edu (N.J. Alvarez).

https://doi.org/10.1016/j.jcis.2019.10.029
0021-9797/© 2019 Elsevier Inc. All rights reserved.

1. Introduction

From an engineering perspective, peptide hydrogels offer a platform with tunable mechanical properties such as rigidity, bioefficacy, and stimuli responsiveness, e.g. the gel can be turned on/off via external stimuli such as pH and temperature [1,2]. Very short, unblocked peptides have the added benefits of biodegradability, scalability, and low production costs [3–7]. While peptide hydrogels remain strong candidates for drug delivery applications and tissue scaffolding, very little is understood regarding the self-assembly of peptides into volume spanning networks [8]. In fact, theories predicting peptide self-assembly into amyloid-type fibrils and/or higher order structures are not complete, and there still remain noteworthy exceptions to the leading hypotheses, such as the unblocked zwitterionic glycyl-histidyl-glycine (GHG) and cationic glycyl-alanyl-glycine (GAG).

The study of peptide self-assembly was originally motivated by the study of amyloid fibrils, which have been implicated in several disorders, such as Parkinson's disease, Huntington's disease, and so-called polyalanine diseases [9–13]. For example, Gazit and coworkers used short peptides as model systems and showed that unblocked dipeptides can self-assemble into supramolecular structures such as fibrils, colloids and nanotubes, depending on the choice of solvent. Moreover, they linked self-assembly to the hydrophobicity of the peptides and specifically the presence of aromatic functions [14–17]. The addition of blocking groups, such as the aromatic Fmoc (fluoroenylmethoxycarbonyl) and *t*-boc (*tert*-butyloxycarbonyl), considerably increased the propensity for self-aggregation [3,18–22]. The fibrillization process could also be achieved by incorporating D-amino acid residues into aromatic tripeptides. However, using D-amino acids and bulky end groups inherently increases the production cost and decreases the sought-after solubility [23].

Some studies have used molecular dynamic simulations to define the propensity for self-aggregation of tri-peptides. For example, Frederix *et al.* worked towards designing rules for a peptide's propensity to form nanostructures under aqueous, pH-neutral conditions [24,25]. They studied all combinations of the twenty common amino acid di- and tripeptides. The peptides were ranked in order of hydrophobicity and aggregation propensity. The result is a weak correlation between the two. Notably, histidine does not have as large of a propensity to aggregate as the other natural aromatic residues, F, Y, and W. Additionally, alanine and glycine were found to exhibit some of the lowest aggregation propensity scores overall. These results further support the hypothesis that for peptides to form a hydrogel, they require alternating or complimentary charges, or a large fraction of aromatic residues [24].

Previously, we have shown that unblocked zwitterionic glycyl-histidyl-glycine (GHG) was shown to form fibrils on the millimeter scale in water upon deprotonation of the imidazole side chain at centimolar concentrations [26]. The most surprising finding was the discovery that cationic glycyl-alanyl-glycine (GAG) forms a strong hydrogel in 55 mol% ethanol/45 mol% water at a peptide concentration of 220 mM [27]. The gel was found to be underlined by a spanning network of crystalline fibrils on a sub-millimeter scale. Vibrational circular dichroism (VCD) revealed two different gel phases, i.e. phase I below 16 °C composed of right-handed twisted fibrils and phase II between 16 °C and the melting temperature at ca. 36 °C comprised of a network of left-handed twisted fibrils above 16 °C [8]. While generally short peptide aggregates form β-sheet tapes [14,18,22,28], the respective wavenumber positions of the amide I' bands indicate that this is not the case for GAG fibrils [27]. Results from density functional theory (DFT) support this notion and suggest that the GAG oligomers can contain a mixture of β-strand, polyproline II, and gamma-turn structures [29]. This goes against the notion that peptide fibrillar structures must exhibit a cross β- sheet structure [22].

More recently, we explored the thermal stability and reformation process of 200 mM GAG in 55 mol% ethanol/45 mol% water [30]. Our results show that the fibrils do not completely reform and are not thermally reversible. GAG hydrogels are highly tunable and subjecting the gel to a temperature above the melting point for various amounts of time and reforming the gel can be used to adjust the final strength of the system. While the peptides self-assembles into fibrils rather quickly (ca. 10–40 min), the fibrillar state is metastable. After sitting for a sufficiently long time at the annealing temperature, the peptides no longer form fibrils when cooled below the transition temperature, and instead form smaller oligomer aggregates whose chirality is determined by the reformation temperature.

Our team initially investigated GAG hydrogels composed of 220 mM GAG in 55 mol% ethanol/45 mol% water. The choice of this mixture occurred more or less by chance, because the gelation process was first observed at these conditions [27]. There are many open questions regarding the thermal stability, thermodynamics, and mechanical properties of GAG hydrogels. For example, the effect of peptide concentration and ethanol fraction on fibrillar network dynamics, and the mechanical properties and thermal stability of final hydrogels have yet to be determined. Indeed, the ability to tune hydrogel properties, such as rigidity, formation kinetics, and melting temperature would be very useful in many biomedical applications, such as drug delivery [31].

In this study, we determine a two-dimensional phase diagram of macroscopic aggregate formation as a function of peptide concentration and ethanol fraction. We used microscopy to study the overall fibril microstructure at steady state along various pathways. We then studied the kinetics of microstructure evolution of the same solutions via rheology. The steady state hydrogels were then melted under a microscope to understand the effect of temperature on microstructure and fibril stability. Moreover, rheology was used to examine the effect of temperature on hydrogel microstructure and fibril connectivity for various peptide concentrations and ethanol fractions. The mechanisms of fibril formation are cast into a solubility framework that captures the observed trends with peptide concentration, ethanol fraction, and temperature. It should be noted that for the sake of readability we focused our efforts on the so-called phase II of the gel which is formed in a temperature region between 16 °C and 30 °C [27].

2. Materials and methods

2.1. Materials

Unblocked glycyl-alanyl-glycine (H-Gly-Ala-Gly-OH) was purchased from Bachem with > 99% purity and used without further purification. The gel samples were prepared by mixing varying amounts of peptide, ethanol (200 proof, Pharmco-Aaper) and deionized water. Hydrochloric acid (ACS grade, Ricca Chemical Company) was added to the solutions to ensure complete protonation of GAG. The protocol for the gel preparation was the following: (1) the appropriate amount of distilled water was added to the peptide powder, (2) the pH was adjusted to around 2 with HCl, and (3) ethanol was added last. The sample was thoroughly mixed after each addition. The final sample solution was clear.

2.2. Gel plate experiment

A systematic experiment was carried out to identify compositions whereby macroscopic fibrils/aggregates were observed. To this end we prepared 96 gel samples with the fraction of ethanol

and concentration of peptide varying simultaneously from one sample to another. The peptide concentration was varied between 50 mM and 350 mM with 25 mM increments. The ethanol fraction ranged from 12 mol% to 100 mol%. The 96-well microplate was monitored over a one-week time period. Fibril formation was indicated by observed macroscopic fibrils using microscopy and the consistency of solution was pasty rather than fluid-like.

2.3. Rheology

Rheology measurements were obtained on a DHR-3 (TA instruments) using a Peltier plate for temperature control with a parallel top plate of diameter 25 mm. 500 to 600 μL of peptide material was deposited on the Peltier plate (held at 20 °C). To avoid solvent evaporation, safflower oil was added as a solvent trap around the free surface of the sample. The ethanol/water solutions were confirmed to have little to no solubility in the oil phase. All samples were prepared one to three minutes prior to loading onto the Peltier plate. Time equal to zero is considered when the ethanol is added to the peptide solution. The exact time between ethanol addition and beginning of the experiment was recorded and accounted for during data treatment. A strain of 0.03%, an angular frequency of 1 rad/s, and a gap of 700 μm were used for the small amplitude oscillatory shear measurements. The storage and loss moduli, and tan δ were recorded as a function of time over a period of a hundred minutes.

Samples for measurement were prepared at constant ethanol fraction of 55 mol% with varying peptide concentration from 100 mM to 300 mM in 50 mM increments to assess the impact of peptide concentration on the kinetics of microstructure evolution. Similarly, to investigate the impact of ethanol fraction, the peptide concentration was set to 200 mM and 300 mM while varying the ethanol fraction from 55 mol% to 74 mol% and from 42 mol% to 64 mol%, respectively. Finally, concentrations of peptide and fractions of ethanol near the sol-gel transition were also studied to assess the simultaneous impact of ethanol fraction and peptide concentration on the gelation kinetics and storage modulus of the gel.

Once the fibril microstructures reached steady state, we performed temperature studies to determine the effect of temperature on fibril microstructure. We used the same small amplitude conditions as before: i.e. 1 rad/s at 0.03% strain. The temperature was raised at a rate of 0.25 °C per minute. The softening point coincides with the "knee" observed in the complex modulus versus temperature plot. To find the precise value, the initial modulus plateau, as well as the region of sharp modulus decrease, were fit by exponential functions (since the traces are linear on a semi-log y plot). The softening temperature is defined as the intersection of the two lines (see Fig. S1). In a second experiment, a 200 mM GAG, 55 mol% ethanol sample was brought from 20 °C to 40 °C in 2 °C increments. After reaching each temperature, the modulus data were collected over a period of 5 min.

2.4. Microscopy

Pictures of the gels were captured on a Nikon Eclipse TE2000-S inverted microscope using the 4X/0.13 Nikon Plan Fluor lens equipped with a Point Grey FL3-U3 camera. Monitoring of the fibrils formation during the gel plate experiment was carried out with an Amscope 7X-45X Trinocular Stereo Zoom microscope equipped with an Amscope Mu130 camera.

3. Results and discussion

3.1. Peptide phase diagram

We determined the critical conditions that caused the self-assembly of cationic GAG into large-scale fibril aggregates as a function of peptide concentration and ethanol fraction. Fig. 1 shows a graphical representation of the 96-well microplate, where the x-axis and y-axis reflect the concentration of peptide and fraction of ethanol, respectively. The samples were formed and monitored over a one-week period and the wells were distinguished visually by noting whether the solution became opaque and visible macroscopic fibrils were observable. The crystalline nature of these fibrils was investigated by wide-angle X-ray scattering. Fig. S2 shows that the gel exhibits an amorphous region, that we attribute to the solvents, and discrete peaks corresponding to the crystallographic planes found in the unit cell of the fibrils. The red-line crossing diagonally through the phase diagram in Fig. 1 is designated the fibril formation phase boundary line where peptide solutions below the line are still stable and above are visually opaque and show macroscopic fibril formation. The asterisks indicate the samples measured in microscopy and rheology.

There are three conclusions that can be drawn by comparing the gels obtained with various compositions. The first is that the previously observed mixture of 220 mM GAG in 55 mol% ethanol/water is close to the fibril transition line [27]. The second is that as concentration of peptide increases, the critical fraction of ethanol to induce the formation of fibrils decreases. Finally, extrapolation of the solubility data (see Fig. S3) suggests insolubility of all peptide concentrations for solutions with $\geq$88 mol% ethanol. For low ethanol fractions, more experiments are necessary to determine whether the curve is diverging, such that below a critical fraction of ethanol all peptide concentrations are in the sol phase.

3.2. Microscope images

A sample of microscopic images of gels obtained in different conditions, indicated in Fig. 1, are analyzed to validate and understand the nature of the fibril microstructure. Fig. 2 shows images of the peptide fibril solutions with the respective conditions indicated below. It is evident that, in all cases, there is a clear formation of very large fibrils. However, different conditions have an effect on the way that the fibrils are packing within solution and thus change the microstructure. For example, the solution of 150 mM GAG in 55 mol% ethanol shows relatively homogeneously dispersed fibrils with a few dense centers. As the peptide concentration increases, the fibril aggregate regions are significantly denser and accompanied by voids. The microstructure is also altered by a change in ethanol fraction (Fig. 2, bottom row). 200 mM of GAG in 55 mol% ethanol shows clusters, but the network spans the whole picture, whereas increasing the fraction of ethanol to 74 mol% induces the formation of a seemingly discontinuous network of very dense fibril regions.

These observations lead to an important hypothesis regarding the interplay between kinetics of fibril formation, and the equilibrium between peptides self-assembling and peptides dissolved in solution. If the solubility of peptide is constant for a given ethanol fraction, then an increase in peptide concentration induces the formation of more fibrils. This hypothesis is supported by the first and second rows of images in Fig. 2, which show higher local density of fibrils for increasing peptide concentration at constant ethanol fraction. The kinetics of peptide self-assembly into fibrils is rather complex, but it can be expected that its rate increases non-linearly with the concentration of peptide dissolved in solution. A higher kinetic rate of fibril formation would lead to less homogeneous packing of fibrils, known as diffusion-limited aggregation in colloidal science [32]. Furthermore, if we argue that the peptide solubility decreases with increasing ethanol fraction, then the higher density of fibrils and decreasing homogeneity observed in the middle and bottom rows of Fig. 2 are explained by more peptides participating in self-assembly.

Fig. 3 shows additional microscopy images that support the above arguments. If the arguments above hold, then similar

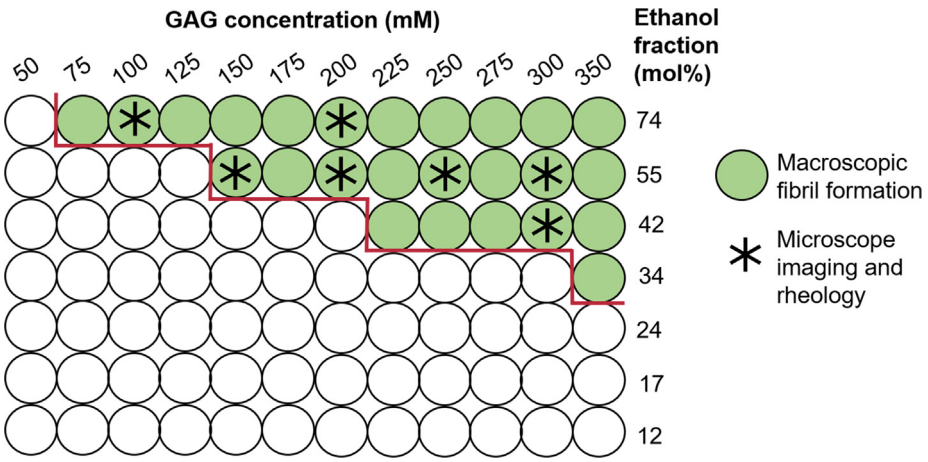

Fig. 1. Phase diagram describing the conditions for visible GAG fibrils at 20 °C.

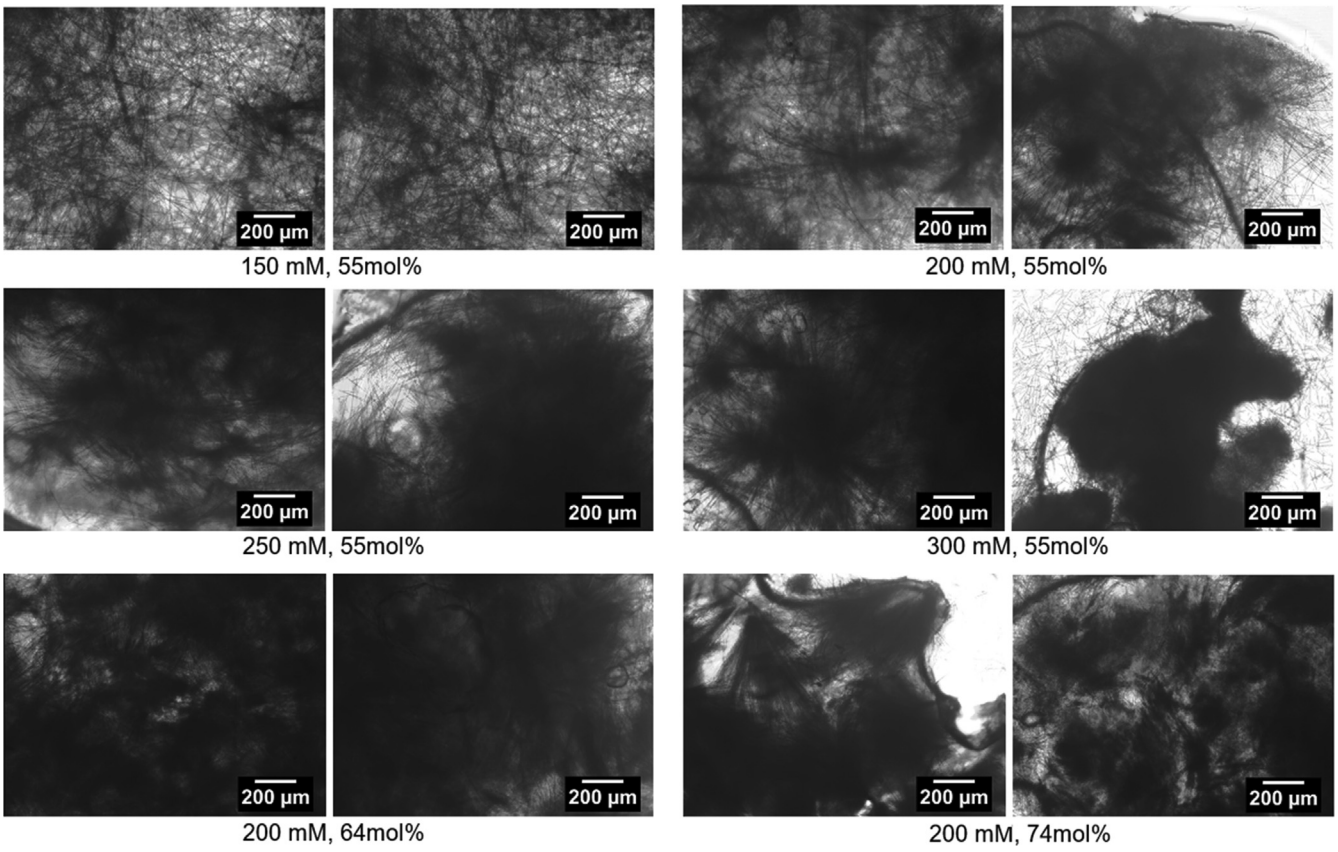

Fig. 2. Microscope images of gels formed at 20 °C with various GAG concentrations and ethanol fractions.

microstructures should be observed by both decreasing peptide concentration and increasing ethanol fraction. For example, Fig. 3a shows long fibrils with spatial gradients in fibril density. Fig. 3b shows a very similar fibril length and packing, but at a lower concentration of peptide and higher fraction of ethanol. Fig. 3c and 3d present a further decrease in peptide concentration and ethanol fraction. The microstructure is less homogeneous which points to faster kinetics. This supports the hypothesis that the fibril microstructure depends on the kinetic rate and concentration of peptide.

The formation of fibrils, potentially leads to a percolated network that induces gel-like properties. Rheology was used to determine whether the formation of fibrils induce a volume spanning network. The different samples that were examined near and across the phase boundary are indicated in Fig. 1.

3.3. Rheology

We used oscillatory shear rheology to probe the microstructure of the macroscopic fibrils in solution. This measurement provides both the elastic, G', and viscous, G'', contributions to the bulk modulus. The formation of a percolated network, i.e. gel, is defined as occurring once the elastic modulus is larger in magnitude than the viscous modulus. The measure of the elastic modulus is inter-

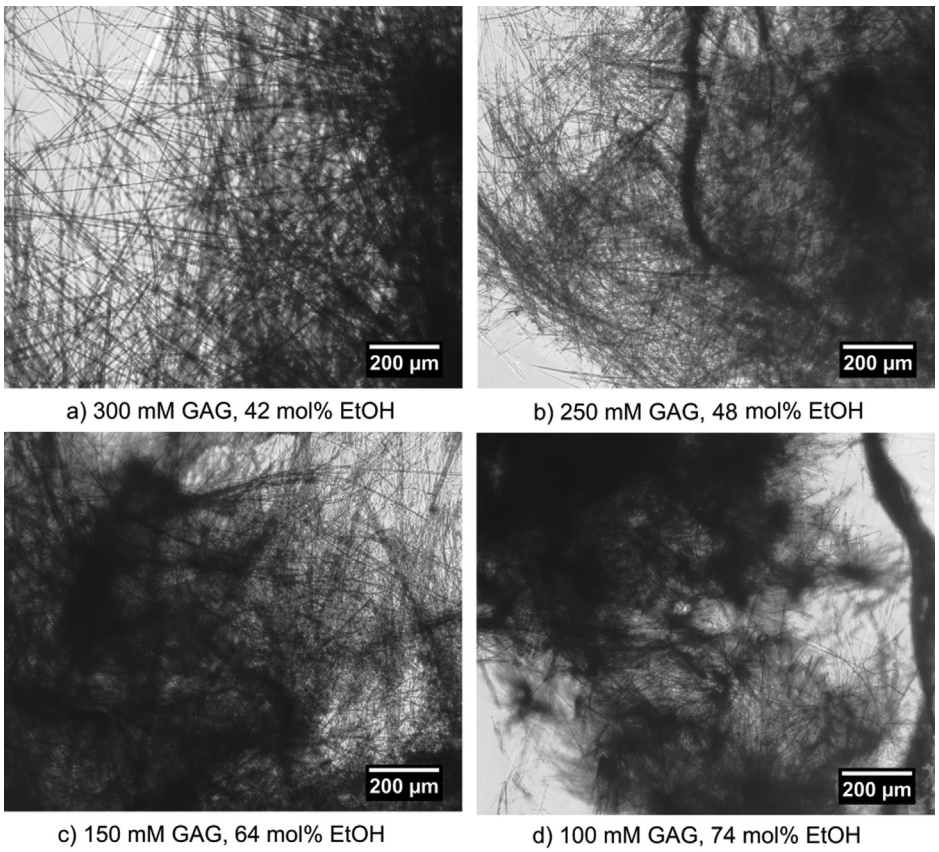

Fig. 3. Microscope images of GAG gels formed at 20 °C.

preted here as the relative connectivity of the network, while the viscous modulus is a measure of the friction between fibrils in the network [33].

One important point is that the nature of fibril formation can lead to kinetic processes that yield the uneven fibril distributions shown in Figs. 2 and 3. Thus, it is not clear whether rheological measurements are reproducible or specific to a particular sample. Therefore, we checked the reproducibility of two sample types: (1) 200 mM GAG in 55 mol% ethanol and (2) 300 mM GAG in 55 mol% ethanol. Note that (1) and (2) were chosen as they represent homogeneous and inhomogeneous microstructure formation, respectively (cf. images in Fig. 2). Fig. S4 shows G' and tan δ as a function of time for triplicates of 200 mM GAG in 55 mol% ethanol. We observe that all three samples have similar initial transient slopes and reach a modulus plateau of similar magnitude; the average steady state storage modulus is 80 ± 26 kPa. There is a larger variability in G' values for the 300 mM GAG gels. Fig. S5 shows G' and tan δ as a function of time for triplicates of 300 mM GAG in 55 mol% ethanol; the average maximum storage modulus is 510 ± 390 kPa. This variability could be due to either the stochastic nature of network formation and the heterogeneities observed in microscopy or to experimental difficulties. Since gelation of these samples is fast, shear and extensional flows imposed on the sample during mixing and loading might have caused the formation of different microstructures and thus different G' values. We conclude that the kinetics measured in rheology are reproducible for quantitative analysis, while steady state G' values vary from sample to sample. Interestingly, the tan δ values derived from G' and G'' exhibit a high degree of reproducibility (Fig. S4) with an average tan δ after 100 min of 0.340 ± 0.008 and 0.358 ± 0.032 for respectively the 200 mM and 300 mM gels.

Fig. 4 shows the effect of varying GAG concentration, ethanol fraction, and both parameters on the kinetics of microstructure formation. Fig. 4a displays the effect caused by a change in GAG concentration. We observed that as the concentration of GAG increases, the rate of microstructure formation increases, suggesting that the concentration of peptide participating in fibrillization increases. Furthermore, at low peptide concentration the gel is significantly weaker than it is for the other cases, suggesting a lower number of fibrils forming with 150 mM GAG. Fig. 4b shows the effect of ethanol fraction on microstructure formation kinetics in log-log scale to accentuate the differences in kinetics. We observe faster kinetics and higher steady state moduli with increasing ethanol fraction. Fig. 4c shows kinetics traces observed by varying both ethanol fraction and peptide concentration. We observed that both variables can be manipulated to achieve similar kinetics of formation for different concentrations of peptide and ethanol fractions. Indeed, if the peptide concentration is low (100 mM) and the ethanol content is high (e.g. 74 mol% ethanol), the time to plateau is similar to the one observed for a sample with 250 mM GAG and 55 mol% ethanol. Furthermore, a sample with high GAG concentration and low ethanol fraction (250 mM GAG, 48 mol% ethanol) has similar kinetics to the 150 mM, 55 mol% ethanol sample. These results are in support of our hypothesis regarding Fig. 3, i.e. slow and fast gelation kinetics yield homogeneous and inhomogeneous microstructures, respectively.

We analyzed the kinetic traces of the storage modulus in terms of a heuristic sigmoidal model, given by:[30]

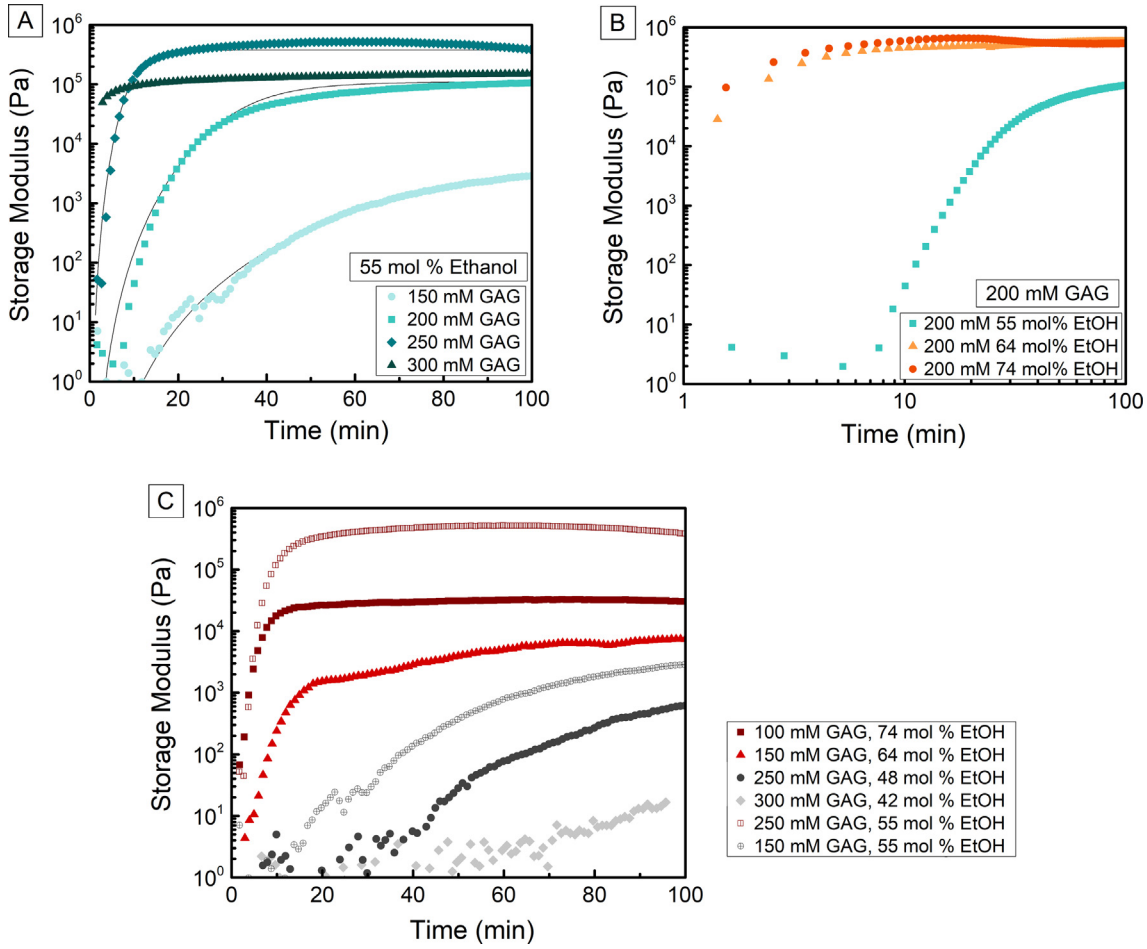

Fig. 4. Storage modulus as a function of time for (a) variations of GAG concentration with fits of Eq. (1) to the experimental data (solid lines), (b) variations of ethanol fraction (log-log plot), and (c) simultaneous variations of GAG concentration and ethanol fraction.

$$G\prime = \frac{G'_{\max}}{1 + \left(\frac{t}{\tau_{gel}}\right)^{a}} \tag{1}$$

where G'_{max} is the maximum or asymptotic value of the storage modulus at long time, τ_{gel} is an effective time constant given by the inflection point of the trace, and a is a measure of the cooperativity of the gelation process. Equation (1) was fit to the kinetic traces in Fig. 4 by using a non-linear least square routine. The parameters and the corresponding statistical errors obtained from fitting equation (1) to the experimental data are listed in Table 1. Note that the value of $1/\tau_{gel}$ is equivalent to a kinetic rate constant of microstructure evolution.

Table 1 lists the obtained time constant and steady state modulus values for the chosen ethanol fractions and peptide concentrations. There is a strong correlation between the kinetic timescale, modulus, and microstructure for the peptide solutions considered. For example, 150 mM and 200 mM in 55 mol% ethanol samples exhibit the most homogeneous microstructures in Fig. 2 and the longest τ_{gel} (i.e. slowest kinetic rates). Furthermore, the time scale decreases (the kinetic rate increases) when increasing the peptide concentration to 250 mM and 300 mM which produces dense clusters of fibrils, see Fig. 2, middle row. This reasoning also applies to an increase of the ethanol fraction from 55 to 74 mol%. We know from observing the formation of fibrils in microscopy that peptides first self-assemble into nuclei that induce the formation of long straight fibrils, see Fig. 5. Fast formation kinetics lead to jamming of growing fibrils and the dense regions observed in Fig. 2, middle and bottom row. This is very similar to clusters that are shown to form during diffusion limited colloidal aggregation (DLCA) in hard sphere self-assembly [34,35]. We also observe that the modulus is a strong function of the microstructure. For example, by increasing the peptide concentration from 150 mM to 300 mM in 55 mol% ethanol, we observe first an increase followed by a decrease of the maximum modulus., The increase most likely arises from the increase in the number of fibrils, while the decrease reflects a loss of homogeneity in the sample volume: dense aggregates with poor inter-connectivity are formed.

The above results support our hypothesis that the number of peptides participating in fibrilization increases with increasing peptide and ethanol fraction. In other words, the rate of gelation/microstructure formation depends on the concentration of peptide and ethanol fraction. GAG is completely insoluble in pure ethanol at room temperature. We prepared a solution with 25 mM GAG in 100 mol% ethanol at 75 °C and observed precipitation when cooled down to 20 °C (see Fig. S6). In 100 mol% water, GAG is soluble in the range of concentrations studied here. Apparently, the addition of ethanol to peptide-water samples lowers the solubility limit of GAG. In other words, for a given ratio of ethanol in water, there is a critical concentration of peptide soluble in solution. From the phase diagram depicted in Figs. 1 and S3, the solubility limit of GAG monomers for a given fraction of ethanol is the phase boundary. Any additional peptide added to solution is free to self-assemble into fibrils. We therefore expect that the rate of gel for-

Table 1
Parameter values obtained from fitting Eq. (1) to the gelation kinetics and tanδ of the obtained hydrogels.

Ethanol fraction (mol%)	GAG concen-tration (mM)	G'_{max} [kPa]	Tan δ_{100min}	τ_{gel} [min]	a
Variations of GAG concentration					
55	150	4.5 ± 0.5	0.26	87.69 ± 0.44	−4.24 ± 0.03
55	200	112.1 ± 0.1	0.34	39.12 ± 0.17	−4.85 ± 0.05
55	250	380.1 ± 1.1	0.48	11.37 ± 0.06	−4.69 ± 0.08
55	300	161.0 ± 1.1	0.36	6.33 ± 0.13	−1.00 ± 0.03
Variations of ethanol fraction					
55	200	112.1 ± 0.1	0.34	39.12 ± 0.17	−4.85 ± 0.05
64	200	562.9 ± 6.5	0.35	3.84 ± 0.06	−2.61 ± 0.10
74	200	535.8 ± 2.6	0.18	2.63 ± 0.02	−2.87 ± 0.04
42	300	–	0.49	–	–
55	300	161.0 ± 1.1	0.31	6.33 ± 0.13	−1.00 ± 0.03
64	300	163.7 ± 1.1	0.34	2.70 ± 0.04	−0.94 ± 0.04
Simultaneous variations of GAG concentration and ethanol fraction					
42	300	–	0.49	–	–
48	250	1.3 ± 0.1	0.25	100.58 ± 1.05	−5.53 ± 0.07
55	200	112.1 ± 0.1	0.34	39.12 ± 0.17	−4.85 ± 0.05
64	150	7.6 ± 0.1	0.23	27.95 ± 0.31	−3.23 ± 0.05
74	100	29.8 ± 0.1	0.28	8.96 ± 0.03	−3.68 ± 0.04

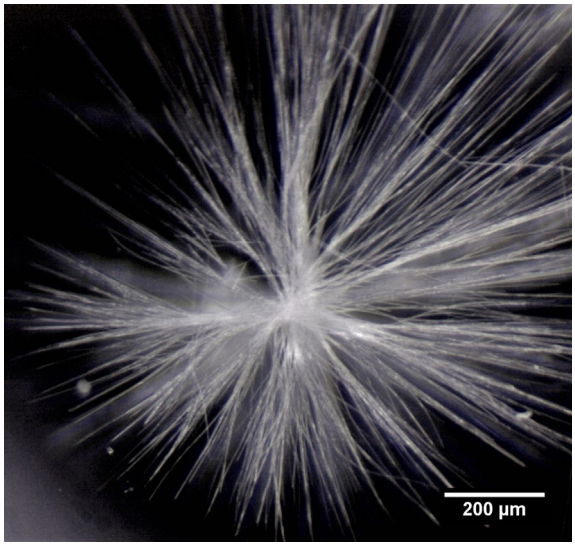

Fig. 5. Microscope image of GAG fibrils formed around an initial nucleus.

mation and growth increases with increasing peptide concentration, as observed in Fig. 4a and Table 1. Furthermore, as the ethanol fraction increases for a given concentration of peptide, the solubility limit decreases; allowing more peptide to participate in self-assembly, ultimately increasing the kinetic rate as observed in Fig. 4b and Table 1. Figs. 3 and 4c validate our arguments since decreasing peptide concentration and increasing ethanol fraction lead to similar rheology kinetics and microstructure.

We previously reported on the thermal reversibility of GAG fibril formation by thermally cycling 200 mM GAG in 55 mol% ethanol. One surprising result was that after melting the fibrils at 50 °C, fewer fibrils formed upon subcooling the solution. In fact, four to five cycles of heating and cooling resulted in the formation of too few fibrils to constitute a volume spanning network. This implies that the formation of the large crystalline fibrils underlying the gel phases of GAG is highly dependent on the initial phase of peptide aggregation in solution. Furthermore, the state of a peptide in solution is temperature dependent. In an attempt to better understand the melting process and how it fits our solubility hypothesis, we performed temperature sweeps to observe the loss of fibril contacts as a function of temperature.

3.4. Effect of temperature

We first observed the fibril network as a function of temperature using microscopy. Fig. 6 shows four images taken at different temperatures for 220 mM peptide in 55 mol% ethanol. As noted above, these conditions produce a rather homogeneous sample spanning network. We observed at increasing temperature a steady decrease in the number of macroscopic fibrils. In other words, as we increased temperature, we increased the solubility of the peptide and the equilibrium shifted to less self-assembled peptide fibrils. At 40 °C, the peptide fibrils were completely dissolved and the solution was clear.

The loss of fibrils was also probed using rheology. Fig. 7 shows the complex modulus as a function of time from 20 °C to 40 °C in 2 °C increments. The complex modulus was chosen as it captures any changes in either G' or G" as a function of temperature. In all cases, we observed an almost immediate drop in modulus and a constant steady state modulus over the observed 5 min measurement window. The complex modulus decreases only slightly up to 24 °C. Then at 26 °C a visible softening occurs followed by a sharp modulus decrease at 28 °C. We were interested in determining the softening point as a function of formation conditions. To this end temperature ramps were conducted at 0.25 °C/min to ensure steady state was reached at each temperature.

Fig. 8 shows the effect of temperature on the fibril microstructure from 20 °C to 65 °C for (a) variations of GAG concentration, (b) ethanol fraction variations and (c) simultaneous variations of GAG concentration and ethanol fraction. We can see that all curves display (1) an initial plateau or quasi-plateau where the complex modulus is slightly decreasing, (2) a "knee" which corresponds to a point where the complex modulus sharply decreases, and (3) a temperature zone where the signal is no longer measurable. Note that none of the gel samples display a clear melting temperature, but rather a continuous spectrum over which G* decreases and the fibrils dissolve back into solution confirming our observations from Figs. 6 and 7. The "knee", which we denote as the softening point temperature T_{soft}, is a point of interest since it marks a large enough loss of fibrils that the modulus becomes a strong function of temperature. We know from microscopy that some fibrils do in fact dissolve below T_{soft}, but it seems not enough fibrils disappear to decrease the modulus.

We analyzed the reproducibility of the complex modulus as a function of temperature for three distinct gel samples. Fig. S7 shows G* as a function of time for 200 mM GAG in 55 mol% etha-

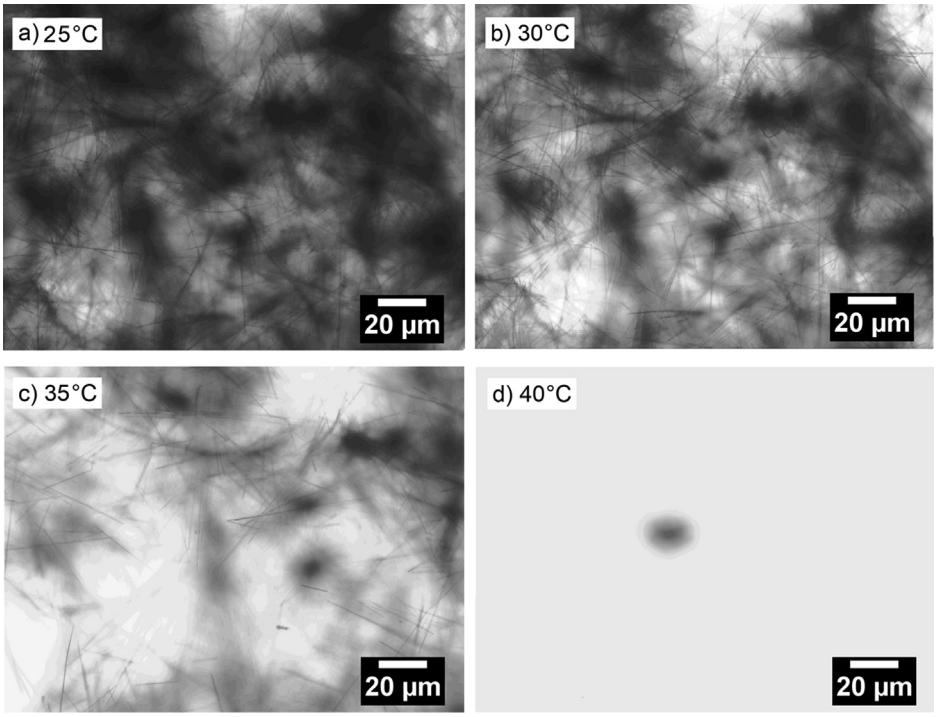

Fig. 6. Microscope images of the progressive melting of a 220 mM GAG and 55 mol% ethanol gel sample.

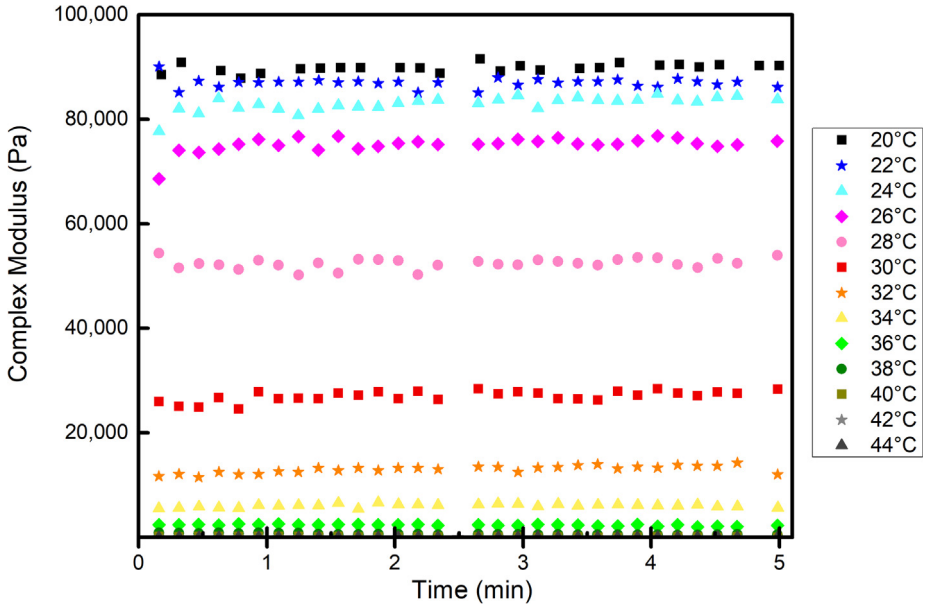

Fig. 7. Complex modulus of a gel with 200 mM GAG and 55 mol % ethanol: 5 min isotherms at increased temperatures from 20 °C to 44 °C.

nol. We observe some variability from sample to sample reflecting the stochastic effects in the melting of the fibrils. The average softening temperature of these triplicates is 24.3 ± 1.4 °C. This is in line with data from Fig. 7, showing an increase in the loss of fibrils after 24 °C.

T_{soft} for the different initial conditions are tabulated in Table 2. Fig. 8 shows that T_{soft} increases with increasing peptide concentration and also with increasing ethanol fraction. Fig. 9 shows a 3D softening point diagram as a function of GAG and ethanol fraction from the data in Table 2. The increase in T_{soft} with increasing ethanol fraction and peptide concentration is clearly visible. Note that by decreasing peptide concentration and increasing ethanol fraction, the softening point remains relatively constant.

The results of these measurements provide direct evidence for the notion that higher peptide concentrations lead to a higher density of fibrils. The observed increase of T_{soft} with increasing peptide concentration and ethanol fraction can be explained in the above introduced solubility framework. If we accept the hypothesis that the solubility limit of GAG in solution depends only on the fraction of ethanol, then higher concentrations of peptide in the same ethanol/water solution result in more peptides self-assembling into fibrils. Furthermore, if we now propose that an increase in temperature increases the solubility limit of GAG, then a more concentrated peptide solution would require a higher temperature to achieve the same concentration of undissolved peptide (peptide fibrils) as a lower concentration of peptide. Likewise, increasing

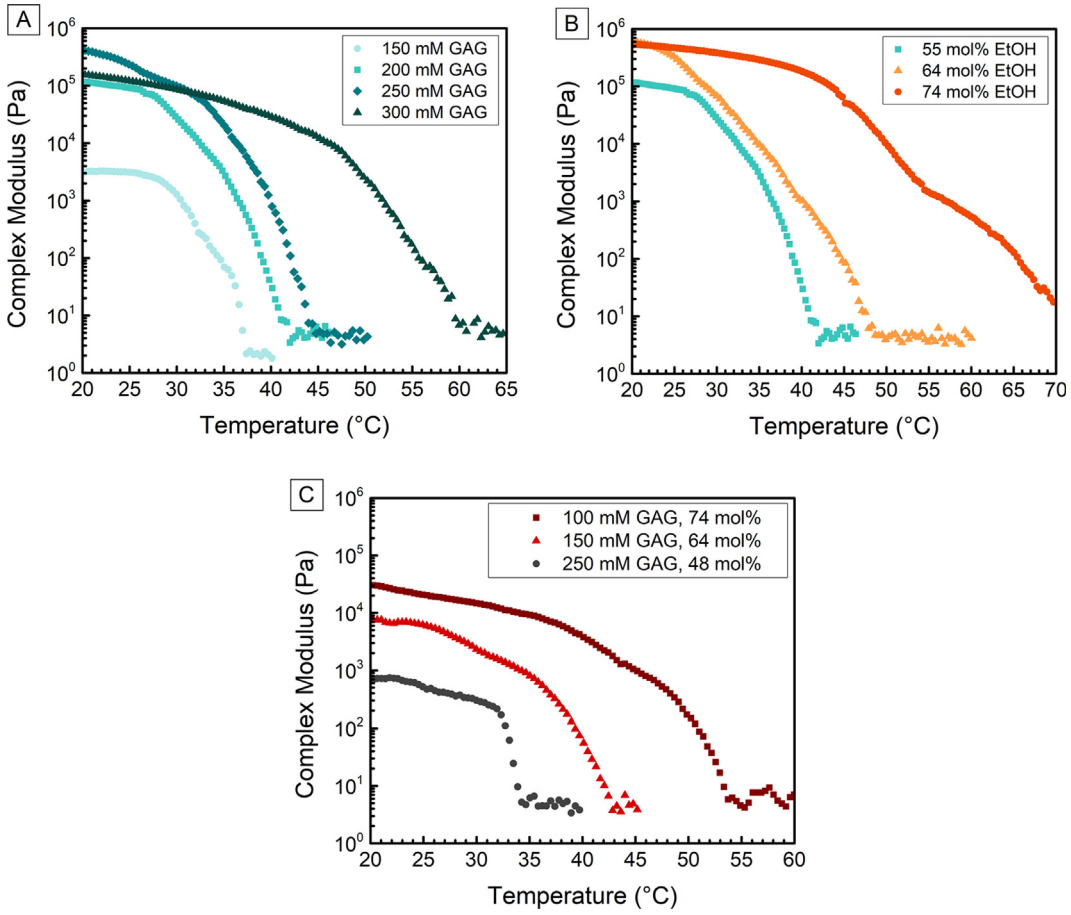

Fig. 8. Complex modulus as a function of temperature for (a) variations of GAG concentration, (b) ethanol fraction and (c) simultaneous variations of GAG concentration and ethanol fraction.

Table 2
Softening temperature of GAG hydrogels obtained by oscillatory rheological measurements for varyiing peptide concentration and ethanol fraction.

	Variations of GAG concentration					
GAG concentration (mM)	150		200	250		300
Ethanol fraction (mol%)	55		55	55		55
Softening point (°C)	28.6		25.4	31.8		46.3
	Variations of ethanol fraction					
GAG concentration (mM)	200	200	200	300	300	300
Softening point (°C)	25.4	24.5	41.2	28.9	46.3	44.0
	Simultaneous variations of GAG concentration and ethanol fraction					
GAG concentration (mM)	300	250	200	150		100
Ethanol fraction (mol%)	42	48	55	64		74
Softening point (°C)	28.9	22.2	25.4	25.4		37.2

ethanol fraction increases undissolved peptide (peptide fibrils) and thus a higher temperature is required to increase the solubility such that a critical number of fibrils (i.e. softening point) is reached. Note that these arguments hinge on the fact that there is a critical number of fibrils at the softening point such that adding more fibrils to solution has a weak effect, and reducing the number of fibrils has a strong effect on G^*. Microscopy measurements strongly indicate that this is the case; however additional quantitative microscopy studies are needed to validate these arguments.

4. Conclusion

The current study provides a fundamental understanding of the self-assembly of GAG into macroscopic fibrils. We argue that much of the phenomena observed can be explained via peptide solubility. Ethanol reduces the solubility of peptide in solution and therefore induces self-assembly at a critical point of peptide concentration and ethanol fraction. The kinetics of fibrilization and microstructure evolution scale with the concentration of peptide available

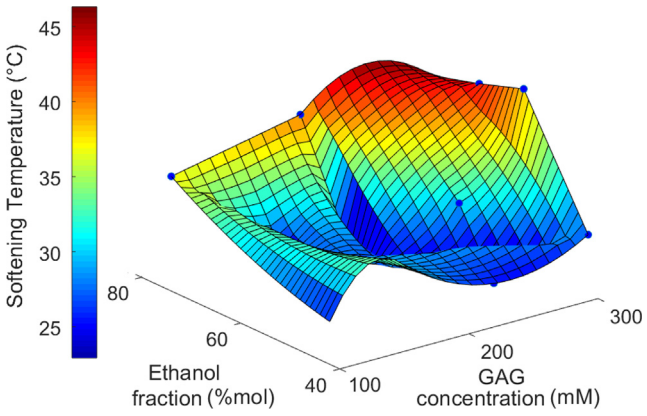

Fig. 9. Three-dimensional phase diagram of the GAG hydrogel representing the softening temperature as a function of GAG concentration and ethanol fraction.

to form fibrils. A higher kinetic rate of fibril formation leads to a less homogeneous packing of fibrils similar to DLCA in colloidal aggregation physics [32,35]. We showed that, via these mechanisms, the initial conditions control the rate of self-assembly, the final fibril density, and the heterogeneity of fibril microstructure. GAG hydrogels can be tailored to form a biomaterial with selected network density, rigidity, rate of gelation, and dissolution temperature [36–39]. We expect that these materials can be optimized to be used as a drug or cell delivery system [40–43] or incorporated in a scaffold for tissue engineering [44–47]. Furthermore, the results here will undoubtedly motivate molecular dynamics simulations [24,25] to better understand the self-assembly process and the importance of ethanol to induce the formation of macroscopic fibrils.

The thermal stability of the gel network is related to solubility dynamics. Increasing solution temperature increases the solubility of peptide in solution and thus reduces the number of fibrils. We showed that there is no critical melt temperature, but a continuous loss of macroscopic fibrils with increasing temperature. We describe a critical temperature T_{soft}, such that the modulus of the fibril network sharply decreases beyond this point. T_{soft} is a strong function of peptide concentration and ethanol fraction. These results demonstrate that GAG hydrogels can be engineered to maintain a modulus above a critical temperature. The development of this material would address the need for delivery systems precisely controlled by temperature [48]. The application of such hydrogels is the focus of future studies.

Acknowledgements

This project is supported by a grant from the National Science Foundation to R.S.S and N.J.A. (DMR-1707770).

Appendix A. Supplementary material

Supplementary data to this article can be found online at https://doi.org/10.1016/j.jcis.2019.10.029.

References

[1] Y. Zhao, H. Yokoi, M. Tanaka, T. Kinoshita, T. Tan, Self-assembled pH-responsive hydrogels composed of the RATEA16 peptide, Biomacromolecules 9 (6) (2008) 1511–1518.
[2] L. Klouda, Thermoresponsive hydrogels in biomedical applications: A seven-year update, Eur. J. Pharm. Biopharm. 97 (2015) 338–349.
[3] L. Adler-Abramovich, E. Gazit, The physical properties of supramolecular peptide assemblies: from building block association to technological applications, Chem. Soc. Rev. 43 (2014) 6881–6893.
[4] W.Y. Seow, C.A.E. Hauser, Short to ultrashort peptide hydrogels for biomedical uses, Mater. Today. 17 (2014) 381–388.
[5] E.R. Draper, D.J. Adams, Low-molecular-weight gels: the state of the art, Chem. 3 (2017) 390–410.
[6] L.J. Dooling, D.A. Tirrell, Peptide and Protein Hydrogels, in: X.J. Loh, O.A. Scherman (Eds.), Monogr. Supramol. Chem. No 11, Royal Society of Chemistry, London, 2013, pp. 93–124.
[7] K.J. Skilling, F. Citossi, T.D. Bradshaw, M. Ashford, B. Kellam, M. Marlow, Insights into low molecular mass organic gelators: a focus on drug delivery and tissue engineering applications, Soft Matter 10 (2014) 237–256.
[8] S. Farrell, D. DiGuiseppi, N. Alvarez, R. Schweitzer-Stenner, The interplay of aggregation, fibrillization and gelation of an unexpected low molecular weight gelator: glycylalanylglycine in ethanol/water, Soft Matter 12 (2016) 6096–6110, https://doi.org/10.1039/c6sm00879h.
[9] C.M. Dobson, Protein misfolding, evolution and disease, Trends Biochem. Sci. 24 (1999) 329–332. http://www.ncbi.nlm.nih.gov/pubmed/10470028.
[10] T.J. Measey, R. Schweitzer-Stenner, Self-assembling alanine-rich peptides of biomedical and biotechnological relevance, 2012. http://doi.org.10.1002/9781118183373.ch11.
[11] M. Levy-Sakin, R. Scherzer-Attali, tein Aggregation-From Nonspecific to Specific Interactions, in: R. Schweitzer-Stenner (Ed.), Protein Pept. Folding, Misfolding Non-Folding, Wiley & Sons, Inc., Hoboken, 2012, pp. 441–478. http://doi.org/QP551.P75.2012.
[12] J. Gsponer, M. Vendruscolo, Theoretical approaches to protein aggregation, Protein Pept Lett. 13 (2006) 287–293. http://www.ncbi.nlm.nih.gov/pubmed/16515457.
[13] R.M. Murphy, Peptide aggregation in neurodegenerative disease, Ann. Rev Biomed. Eng. 4 (2002) 155–174, https://doi.org/10.1146/annurev.bioeng.4.092801.094202.
[14] E. Gazit, Self assembly of short aromatic peptide into amyloid fibrils and related nanostructures, Prion. 1 (2007) 32–35.
[15] M. Reches, Y. Porat, E. Gazit, Amyloid fibril formation by pentapeptide and tetrapeptide fragments of human calcitonin, J. Biol. Chem. 277 (2002) 35475–35480.
[16] M. Reches, E. Gazit, Formation of closed-cage nanostructures by self-assembly of aromatic dipeptides, Nano Letters 4 (2004) 581–585, https://doi.org/10.1021/nl035159z.
[17] G. Colombo, P. Soto, E. Gazit, Peptide self-assembly at the nanoscale: a challenging target for computational and experimental biotechnology, Trends Biotechnol. 25 (2007) 211–218.
[18] R. Orbach, I. Mironi-Harpaz, L. Adler-Abramovich, E. Mossou, E.P. Mitchell, V.T. Forsyth, E. Gazit, D. Seliktar, The rheological and structural properties of fmoc-peptide-based hydrogels: the effect of aromatic molecular architecture on self-assembly and physical characteristics, Langmuir 28 (2012) 2015–2022.
[19] L. Adler-Abramovich, L. Vaks, O. Carny, D. Trudler, A. Magno, A. Caflish, D. Frenkel, E. Gazit, Phenylalanine assembly into toxic fibrils suggests amyloid etiology in phenylketonuria, Nat. Chem. Biol. 8 (2012) 701–706.
[20] C. Tang, A.M. Smith, R.F. Collins, R.V. Ulijn, A. Saiani, Fmoc-diphenylalanine self-assembly mechanism induces apparent pK_a shifts, Langmuir 25 (2009) 9447–9453.
[21] A.M. Smith, R.J. Williams, C. Tang, P. Coppo, R.F. Collins, M.L. Turner, A. Saiani, R.V. Ulijn, Fmoc-diphenylalanine self-assembles to a hydrogel via a novel architecture based on pi-pi interlocked beta sheets, Adv. Matter. 20 (2008) 37–38.
[22] S. Fleming, P.W.J.M. Frederix, I.R. Sasselli, N.T. Hunt, R.V. Ulijn, T. Tuttle, Assessing the utility of infrared spectroscopy as a structural diagnostic tool for β-sheets in self-assembling aromatic peptide amphiphiles, Langmuir 29 (2013) 9510–9518.
[23] S. Marchesan, C.D. Easton, K.E. Styan, L.J. Waddington, F. Kushaki, L. Gooddall, K.M. McLean, J.S. Forsythe, P.G. Hartely, Chirality effects at each amino acid position on tripeptide self-assembly into hydrogel bio-materials, Nanoscale 6 (2014) 5172–5180.
[24] P.W. Frederix, G.G. Scott, Y.M. Abul-Haija, D. Kalafatovic, C.G. Pappas, N. Javid, N.T. Hunt, R.V. Ulijn, T. Tuttle, Exploring the sequence space for (tri-)peptide self-assembly to design and discover new hydrogels, Nat Chem. 7 (2015) 30–37, https://doi.org/10.1038/nchem.2122.
[25] P.W.J.M. Frederix, R.V. Ulijn, N.T. Hunt, T. Tuttle, Virtual screening for dipeptide aggregation: toward predictive tools for peptide self-assembly, J. Phys. Chem. Lett. 2 (2011) 2380–2384.
[26] D. DiGuiseppi, R. Schweitzer-Stenner, Probing conformational propensities of histidine in different protonation states of the unblocked glycyl-histidyl-glycine peptide by vibrational and NMR spectroscopy, J. Raman Spectrosc. 47 (2016) 1063–1072, https://doi.org/10.1002/jrs.4885.
[27] B. Milorey, S. Farrell, S.E. Toal, R. Schweitzer-Stenner, Demixing of water and ethanol causes conformational redistribution and gelation of the cationic GAG tripeptide, Chem Commun. 51 (2015) 16498–16501, https://doi.org/10.1039/c5cc06097d.
[28] R.V. Ulijn, N. Bibi, V. Jayawarna, P.D. Thornton, S.J. Todd, R.J. Mart, A.M. Smith, J. E. Gough, Bioresponsive hydrogels, Mater. Today. 10 (2007) 40–48.
[29] N.V. Ilawe, R. Schweitzer-Stenner, D. DiGuiseppi, B.M. Wong, Is a cross-β-sheet structure of low molecular weight peptides necessary for the formation of fibrils and peptide hydrogels, Phys. Chem. Chem. Phys. 20 (2018) 18158–18168.

[30] D. DiGuiseppi, L. Thursch, N.J. Alvarez, R. Schweitzer-Stenner, Exploring the thermal reversibility and tunability of a low molecular weight gelator using vibrational and electonic spectroscopy and rheology, Soft Matter 12 (2019) 6096–6110.
[31] C. Yan, D.J. Pochan, Rheological propensities of peptide-based hydrogels for biomedical and other applications, Chem. Soc. Rev. 39 (2010) 3528–3540.
[32] W.C.K. Poon, M.D. Haw, Mesoscopic structure formation in colloidal aggregation and gelation, Adv. Colloid Interface Sci. 73 (1997) 71–126, https://doi.org/10.1016/S0001-8686(97)90003-8.
[33] F.C. MacKintosh, J. Käs, P.A. Jammey, Elasticity of semiflexible biopolymer network, Phys. Rev. Lett. 75 (1995) 4425–4428.
[34] D.A. Weitz, J.S. Hunag, M.Y. Lim, J. Sung, Dynamics of diffusion-limited kinetic aggregation, Phys. Rev. Lett. 53 (1984) 1657–1660.
[35] A. Zaccone, H.H. Winter, M. Siebenbürger, M. Ballauf, Linking self-assembly, rheology, and gel transition in attractive colloids, J. Rheol. 58 (2014) 1219–1244.
[36] E.R. Draper, K.L. Morris, M.A. Little, J. Raeburn, C. Colquhoun, E.R. Cross, T.O. McDonald, L.C. Serpell, D.J. Adams, Hydrogels formed from Fmoc amino acids, Cryst. Eng. Comm. 17 (2015) 8047–8057.
[37] B. Ozbas, J. Kretsinger, K. Rajagopal, J.P. Schneider, D.J. Pochan, Salt-triggered peptide folding and consequent self-assembly into hydrogels with tunable modulus, Macromolecules 37 (2004) 7331–7337.
[38] A. Aggeli, M. Bell, L.M. Carrick, C.W.G. Fishwick, R. Harding, P.J. Mawer, S.E. Radford, A.E. Strong, N. Boden, pH as a trigger of peptide β-sheet self-assembly and reversible switching between nematic and isotropic phases, J. Am. Chem. Soc 125 (2003) 9619–9628.
[39] M. Suzuki, M. Yumoto, M. Kimura, H. Shirai, K. Hanabusa, A family of low-molecular-weight hydrogelators based on L-lysine derivatives with a positively charged terminal group, Chem. Eur. J. 9 (2003) 348–354.
[40] M.C. Branco, D.J. Pochan, N.J. Wagner, J.P. Scneider, Macromolecular diffusion and release from self-assembled β-hairpin peptide hydrogels, Biomaterials 30 (2009) 1339–1347.
[41] M.R. Reithofer, K. Chan, A. Lakshmanan, D.H. Lam, A. Mishra, B. Gopalan, M. Joshi, S. Wang, C.A.E. Hauser, Ligation of anti-cancer drugs to self-assembling ultrashort peptides by click chemistry for localized therapy, Chem. Sci. 5 (2014) 625–630.
[42] E.L. Bakota, Y. Wang, F.R. Danesh, J.D. Hartgerink, Injectable multidomain peptide nanofiber hydrogel as a delivery agent for stem cell secretome, Biomacromolecules 12 (2011) 1651–1657.
[43] L. Haines-Butterick, K. Rajagopal, M. Branco, D. Salick, R. Rughani, M. Pilarz, M. S. Lamm, D.J. Pochan, J.P. Schneider, Controlling hydrogelation kinetics by peptide design for three-dimensional encapsulation and injectable delivery of cells, Proc. Natl. Acad. Sci. 104 (2007) 7791–7796.
[44] V. Jayawarna, S.M. Richardson, A.R. Hirst, N.W. Hodson, A. Saiani, J.E. Gough, R. V. Ulijn, Introducing chemical functionality in Fmoc-peptide gels for cell culture, Acta Biomater. 5 (2009) 934–943.
[45] M. Zhou, A.M. Smith, A.K. Das, N.W. Hodson, R.F. Collins, R.V. Ulijn, J.E. Gough, Self-assembled peptide-based hydrogels as scaffolds for anchorage-dependent cells, Biomaterials 30 (2009) 2523–2530.
[46] J. Kisiday, M. Jin, B. Kurz, H. Hung, C. Semino, S. Zhang, A.J. Grodzinsky, Self-Assembling peptide hydrogel fosters chondrocyte extracellular matrix production and cell division: implications for cartilage tissue repair, Proc. Natl. Acad. Sci. 15 (2002) 9996–10001.
[47] D.A. Harrington, E.Y. Cheng, M.O. Guler, L.K. Lee, J.L. Donovan, R.C. Claussen, S.I. Stupp, Branched peptide-amphiphiles as self-assembling coatings for tissue engineering scaffolds, Biomed. Mater. Res., Part A 78 (2006) 157–167.
[48] T.R. Hoare, D.S. Kohane, Hydrogels in drug delivery: Progress and challenges, Polymer 49 (2008) 1993–2007.